

# UCSF

## UC San Francisco Previously Published Works

### Title

Aberrant cortical spine dynamics after concussive injury are reversed by integrated stress response inhibition

### Permalink

<https://escholarship.org/uc/item/9wx9s5v8>

### Journal

Proceedings of the National Academy of Sciences of the United States of America, 119(42)

### ISSN

0027-8424

### Authors

Frias, Elma S  
Hoseini, Mahmood S  
Krukowski, Karen  
[et al.](#)

### Publication Date

2022-10-18

### DOI

10.1073/pnas.2209427119



### Copyright Information

This work is made available under the terms of a Creative Commons Attribution License, available at <https://creativecommons.org/licenses/by/4.0/>

Peer reviewed



# Aberrant cortical spine dynamics after concussive injury are reversed by integrated stress response inhibition

Elma S. Frias<sup>a,b,1</sup>, Mahmood S. Hoseini<sup>c</sup>, Karen Krukowski<sup>a,b,1</sup>, Maria Serena Paladini<sup>a,b,1</sup>, Katherine Grue<sup>a,b,1</sup>, Gonzalo Ureta<sup>d</sup>, Kira D. A. Rienecker<sup>a,b</sup>, Peter Walter<sup>e,f,1,2</sup> , Michael P. Stryker<sup>c,g,2</sup> , and Susanna Rosji<sup>a,b,g,h,i,1,2</sup>

Contributed by Michael P. Stryker; received June 2, 2022; accepted September 9, 2022; reviewed by Cesar Borlongan and Joshua Trachtenberg

Traumatic brain injury (TBI) is a leading cause of long-term neurological disability in the world and the strongest environmental risk factor for the development of dementia. Even mild TBI (resulting from concussive injuries) is associated with a greater than twofold increase in the risk of dementia onset. Little is known about the cellular mechanisms responsible for the progression of long-lasting cognitive deficits. The integrated stress response (ISR), a phylogenetically conserved pathway involved in the cellular response to stress, is activated after TBI, and inhibition of the ISR—even weeks after injury—can reverse behavioral and cognitive deficits. However, the cellular mechanisms by which ISR inhibition restores cognition are unknown. Here, we used longitudinal two-photon imaging *in vivo* after concussive injury in mice to study dendritic spine dynamics in the parietal cortex, a brain region involved in working memory. Concussive injury profoundly altered spine dynamics measured up to a month after injury. Strikingly, brief pharmacological treatment with the drug-like small-molecule ISR inhibitor ISRIB entirely reversed structural changes measured in the parietal cortex and the associated working memory deficits. Thus, both neural and cognitive consequences of concussive injury are mediated in part by activation of the ISR and can be corrected by its inhibition. These findings suggest that targeting ISR activation could serve as a promising approach to the clinical treatment of chronic cognitive deficits after TBI.

*in vivo* two-photon imaging | closed-head injury | integrated stress response | dendritic spine | mouse parietal cortex

Traumatic brain injury (TBI) is defined as the disruption of normal brain function after an impact (a bump, blow, or jolt) to the head that produces direct damage from mechanical forces and indirect damage from secondary responses. Between 1.5 and 3.8 million people experience TBI each year in the United States alone (1, 2). At least 75% of TBI-diagnosed injuries are considered “mild” (defined as concussive injuries without loss of consciousness) (1). TBI is a serious health concern due to chronic behavioral and cognitive impairments that affect the quality of life of millions of individuals (3–6). TBI is also the strongest environmental risk factor for the development of dementia (3, 4). While preclinical experimental studies are steadily increasing, little is known about the cell-specific changes in the brain that are responsible for the persistent cognitive deficits that develop after even mild TBI. With no identified mechanisms, there are no treatments to prevent or mitigate deficits resulting from TBI.

The closed-head injury (CHI) mouse model for TBI produces cognitive deficits comparable to those observed after concussive injuries in humans, such as working memory dysfunction (7). A type of working memory, known as short-term memory, is dependent on multiple cortical regions, including prefrontal and parietal cortex (8–10). All types of memory (including short-term memory) are thought to be encoded in connections among neurons at synapses (11–13). Most excitatory synapses connect to excitatory neurons via dendritic spines, which are specialized protuberances containing the postsynaptic receptors for neurotransmitters (14). Different types of cortical neurons have between 100 and a few thousand dendritic spines. Memory (both formation and maintenance) depends on synaptic plasticity (i.e., the capacity of synapses to undergo lasting biochemical and morphological changes in strength in response to neuronal activity and neuromodulators). Changes in synaptic plasticity are associated with lasting changes in the structure of dendritic spines (structural plasticity) (15–17).

Dendritic spines consist of a spine head connected to the dendritic shaft by a spine neck (18). When stable, functional synapses are connected, dendritic spines may be stable for months to years. Functional synapses are associated with dendritic spines that have a bulbous spine head, as they harbor neurotransmitter receptors, intracellular signaling molecules, ribosomes that mediate local protein synthesis, and a highly active cytoskeleton meshwork (19, 20). Spine necks are barriers that filter the electrical

## Significance

After traumatic brain injury, temporary pharmacological inhibition of the integrated stress response (ISR) with a small-molecule inhibitor (ISRIB) rescued long-lasting trauma-induced cognitive deficits. Here, we found that ISRIB treatment rapidly and persistently reversed the aberrant changes in cortical spine dynamics in the parietal cortex while rescuing working memory deficits. These data suggest that the link between the ISR and memory function involves, at least in part, changes in neuronal structure. Targeting ISR activation could serve as a promising approach to the clinical treatment of chronic cognitive deficits after brain injuries.

Author contributions: E.S.F., M.S.H., K.K., M.P.S., and S.R. designed research; E.S.F., M.S.H., M.S.P., G.U., and K.D.A.R. performed research; E.S.F., K.K., M.S.P., K.G., P.W., M.P.S., and S.R. analyzed data; and E.S.F., P.W., M.P.S., and S.R. wrote the paper.

Reviewers: C.B., University of South Florida Center of Excellence for Aging and Brain Repair; and J.T., University of California, Los Angeles.

Competing interest statement: P.W. has a patent application for the invention of ISRIB. Rights to the invention have been licensed by the University of California, San Francisco, to Calico.

Copyright © 2022 the Author(s). Published by PNAS. This open access article is distributed under Creative Commons Attribution License 4.0 (CC BY).

<sup>1</sup>Present address: Bay Area Institute of Science, Altos Labs, 2400 Bridge Parkway, Redwood City, CA 94065.

<sup>2</sup>To whom correspondence may be addressed. Email: pwalter@altoslabs.com, michael.stryker@ucsf.edu, or srosi@altoslabs.com.

This article contains supporting information online at <http://www.pnas.org/lookup/suppl/doi:10.1073/pnas.2209427119/-DCSupplemental>.

Published October 13, 2022.

component of synaptic signals and amplify spine head depolarization, as well as limit the diffusion of intracellular messengers from the spine head into the dendrite (21).

Dendritic spines have captured the attention of neuroscientists for over 100 y because they are the elements of synaptic connectivity that are visible in the light microscope. Spines are characterized by their dynamics, that is, their structural plasticity, density, and morphology. Spine structural plasticity describes the formation and elimination of spines that take place over hours or days, which is important for the development and proper function of the central nervous system (19, 22–24). Spine density is measured as the number of spines per measured length of dendrite and is used as a measure of the total synaptic strength received by a dendrite (18). Spine morphology describes the shape and size of dendritic spines (25, 26). The regulation of each of these factors is essential for stable synaptic maintenance and transmission and thus cognitive and executive function, such as working memory (16, 17, 23, 24).

Pioneering work from Lendvai et al., Grutzendler et al., Trachtenberg et al., and Holtmaat et al. (27–30) in the early 2000s demonstrated that it was possible to track the same spine in the living brain over a long period of time using two-photon imaging *in vivo*. From such time-lapse imaging studies, a new picture of spines began to emerge. Dendritic spines could be seen *in vivo* to change their shape and size (morphology), to form or disappear across an animal's life span (dynamics), and to be responsive to the animals' experience and environment. Later studies have shown that spine morphology and dynamics vary among neuronal types and across developmental stages (31). The balance between spines forming or disappearing determines spine density. Currently, changes in spine morphology, dynamics, and density are accepted markers for changes in synaptic strength or synaptic presence.

The integrated stress response (ISR) is a universally conserved intracellular signaling network that responds to a variable environment to maintain homeostasis (32, 33). Four specialized kinases (PERK [PKR-like ER kinase], PKR [double-stranded RNA-dependent protein kinase], GCN2 [general amino acid control nonderepressible], and HRI [heme-regulated inhibitor 2]) converge on the phosphorylation of a single serine on the  $\alpha$  subunit of the translation initiation factor eIF2 (33, 34). PERK, PKR, and GCN2 are expressed in the mammalian brain (34). The phosphorylation-mediated central regulatory step leads to a reduction in global protein translation and to the translational up-regulation of a select subset of messenger RNAs, such as activating transcription factor 4 (32, 34). ISR-mediated reprogramming of translation maintains or reestablishes physiological homeostasis; however, chronic ISR activation can also create

maladaptive cellular and functional changes (35). Previous work from our laboratory demonstrated that pharmacological inhibition of the ISR using the drug-like small-molecule ISR inhibitor (ISRIB) is sufficient to reverse electrophysiological impairments, as well as chronic cognitive and behavioral deficits in different rodent TBI models (36, 37). The cellular mechanisms by which ISR inhibition restores neuronal function—and ultimately cognitive function—remain unknown. In the current study, we used longitudinal two-photon imaging *in vivo* to reveal cortical spine dynamics weeks after a single mild closed-head concussive injury and measured the effect of temporary ISR inhibition on both spine dynamics and working memory.

## Results

**Concussive Injury Alters Cortical Spine Dynamics.** To determine the effect of concussive injury on spine dynamics and density, we performed longitudinal transcranial two-photon imaging *in vivo* using Thy1-YFP-H transgenic mice. In this transgenic mouse line, YFP is expressed in a small subset of layer V pyramidal neurons that extend their apical dendrites to layer I/II of the cortex (38). We first subjected mice to a single mild concussive CHI, a reproducible and translational model for concussive injury (39). To perform CHI, animals were secured to a stereotaxic frame with nontraumatic ear bars. We surgically exposed the skull and induced a single bilateral closed-head impact injury with a pneumatic piston over the parietal cortex. No animals had a fractured skull after injury. After impact, the scalp was sutured. Sham controls received the same surgery but no impact. This concussive injury produced no changes in neuronal numbers in the parietal cortex, as measured by quantification of NeuN-positive neuronal nuclei (*SI Appendix, Fig. S1*). Eight days later, we implanted a head fixation device and cranial window directly above the parietal cortex (encompassing the impacted region).

To collect longitudinal data on dendritic spines, we imaged apical dendritic segments for four or five sessions over 8 to 15 d (starting at day 11 post-CHI or post-sham surgery), with the final imaging on day 25 (green arrowheads in Fig. 1). We analyzed each dendritic segment independently and imaged between 40 and 57 segments in each of the imaging sessions. We first quantified the number of spines per dendrite on day 11 (first imaging session) and then identified new spines present on days 13, 15, 18, and 25 (subsequent imaging sessions). To this end, we gave each spine a unique identifier (represented by X, Y, Z coordinates). Similarly, we next quantified the number of spines per dendrite on day 11 and asked whether these spines were still

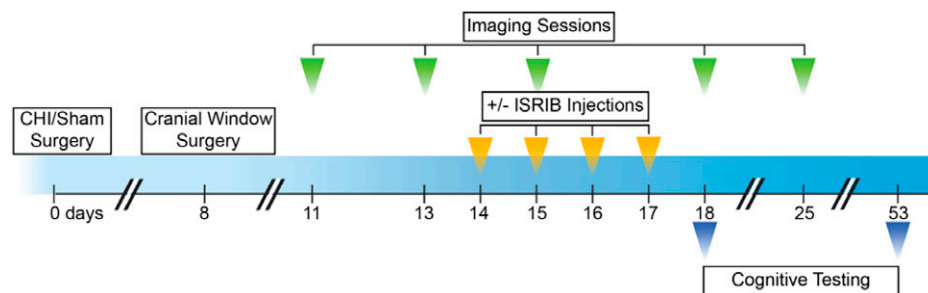


**Fig. 1.** Schematic representation of experiment design. Experimental design for surgeries, imaging,  $\pm$  ISRIB treatment paradigm, and cognitive testing. For the imaging experiments, adult Thy1-YFP-H transgenic male mice were subjected to CHI or sham surgery (day 0). On day 8 a head fixation device and cranial window was implanted directly above the parietal cortex (encompassing the impacted region). Mice were imaged for four to five sessions starting at day 11 with the final imaging day on days 18 or 25. Mice received four daily intraperitoneal injections of ISRIB or Vehicle (2.5 mg/kg) starting on day 14. For the cognitive testing, adult WT male mice were first subjected to CHI or sham surgery (day 0), then received  $\pm$  ISRIB treatment starting on day 14, and lastly underwent cognitive testing on days 18 and 53.

present on subsequent imaging sessions. Based on these measurements, we defined (i) “spine formation” as the fraction of new spines formed in a new location and (ii) “spine elimination” as the fraction of preexisting spines eliminated, both measurements in reference to baseline day 11 (Fig. 2*A*). Representative images for these analyses are shown in Fig. 2*B*. The persistence of the dendritic spines identified was not considered in the analysis of spine formation and elimination but are further discussed in Fig. 3.

In a few cases (<30%) in which a spine appeared to be eliminated but reappeared in a subsequent session in the same location, that spine was counted as if it were a reappearance of the original spine. We counted all protrusions from the dendrites greater than 0.55  $\mu\text{m}$  in length as spines regardless of their morphology. In total, we analyzed a length of at least 3,500  $\mu\text{m}$  of dendrites (each 50 to 100  $\mu\text{m}$  [ $\pm 2 \mu\text{m}$ ]) in length per mouse, amounting to 200 to 600 spines per experimental group. Analysis was done semiautomated, blinded to treatment and surgical condition, and was cross-checked by a separate investigator. Data reported are the average of the counts by multiple investigators. A detailed summary of the data sampling is listed in *SI Appendix, Table S1*.

At 13 d postinjury, mice that received a CHI showed a significant increase in spine formation compared with control mice that received sham surgery. This increase in spine formation was observed between each subsequent imaging sessions. As expected, control mice maintained a ratio of  $\sim 0.2$  new spines formed per preexisting spine (40), which increased to  $\sim 0.5$  after injury (compare bars 1 and 2, Fig. 2 *C–F*). In contrast to their significant increase in spine formation, mice that received a CHI showed no significant change in spine elimination compared with control mice (compare bars 1 and 2, Fig. 2 *G–J*). We further validated these conclusions and excluded that any measured changes were due to phototoxicity by reverse-time analysis, using day 18 as the baseline imaging day (*SI Appendix, Fig. S2*). We concluded that concussive injury massively increases spine formation. As we show below, many of these newly formed spines are transient and are quickly eliminated and, as such, do not factor into our spine elimination score, which scores changes in preexisting spines from baseline images.

**ISR Inhibition Persistently Reverses the Aberrant Spine Dynamics Measured after Concussive Injury.** We previously showed that ISR inhibition alleviates cognitive deficits after CHI (36, 37). Therefore, we next tested whether pharmacological blockage of the ISR using the drug-like small-molecule ISR inhibitor ISRIB would modify the aberrant spine dynamics observed after CHI. To this end, we administered ISRIB (or vehicle) on 4 consecutive d starting at day 14 post-CHI or post-sham surgery (yellow arrowheads in Fig. 1). ISRIB concentrations in the brain measured at 3 and 17 h following the last injection were consistent with earlier findings (*SI Appendix, Fig. S3*) (41).

We observed that at day 15, only 1 d after the first injection, spine formation in CHI mice that received ISRIB treatment was restored toward control levels and was maintained similar to control levels thereafter (compare bars 2 and 3, Fig. 2 *C–F*). Importantly, we observed no effects of ISRIB treatment on spine measurements in control mice that received sham surgery (compare bars 1 and 2 for days 15 to 25, *SI Appendix, Fig. S4*). In contrast to its effect on spine formation, ISRIB treatment only modestly affected spine elimination (Fig. 2 *G–J*). As above, these relationships were also observed in the reverse-time analysis using day 18 as the baseline imaging day (*SI Appendix, Fig. S2*). Thus, ISRIB treatment reversed the CHI-induced increase in spine formation back to the levels of uninjured mice. This restorative

effect persisted for at least 1 wk after ISRIB treatment was ended on day 17 postinjury (compare bars 2 and 3, Fig. 2*F*), that is, long after the drug [ $T_{1/2} \sim 8 \text{ h}$  (41)] had cleared from the system.

From the longitudinal data, we also measured spine density, calculated as the number of spines per micrometer of dendritic length, and observed no significant differences among groups (Sham  $\pm$  ISRIB; CHI  $\pm$  ISRIB) (*SI Appendix, Fig. S8*).

**ISR Inhibition Normalizes the CHI-Induced Short-Lived Newborn Spines.** We next used the longitudinal data to examine the persistence of the new spines formed after concussive injury and whether they were long- or short-lived. We defined (i) “long-lived” as new spines that appeared and remained in place for each subsequent imaging session and (ii) “short-lived” as new spines that appeared but disappeared at subsequent imaging sessions. In some cases (<10%) in which a spine appeared to be eliminated but reappeared in a subsequent session in the same location, that spine was considered short-lived. To this end, we first counted all newly formed dendritic spines at days 13, 15, 18, and 25 (Fig. 3*A*). In each imaging session, we observed a similar number of newly generated spines per dendritic segment that was approximately three- to fourfold greater in animals that received a CHI (red curve) than in those that received sham surgery (light blue curve). The dendritic segment lengths analyzed were similar among groups (*SI Appendix, Table S1*). Remarkably, over the time course of ISRIB treatment, the number of newly formed spines normalized to control levels (dark blue curve) (Fig. 3*B*). ISRIB treatment had no effect on the persistence of new spines in control animals (Fig. 3*B*).

Statistical analysis confirmed that CHI mice had significantly more newly formed spines per dendritic segment than controls at each imaging session ( $P < 0.0001$ ,  $P < 0.05$ ,  $P < 0.005$ ,  $P < 0.0005$ , for imaging sessions 13, 15, 18, and 25 respectively). Conversely, ISRIB treatment of CHI animals significantly reduced newly formed spines, which became statistically indistinguishable from controls ( $P = 0.371$ ,  $P = 0.440$ ,  $P = 0.803$ ) (*SI Appendix, Fig. S5*). Thus, taken together, the data in Fig. 3 strongly suggest that most newly formed spines are short-lived.

To further test this conjecture, we determined the stability of each newly formed spine by noting whether it persisted in subsequent imaging sessions and calculating a “survival index,” in which a value closer to 1 denotes a larger fraction of long-lived spines and a value closer to 0 denotes a larger fraction of short-lived spines (42). New spines born between days 11 and 13 had a survival index of  $\sim 0.9$  in control animals when observed at day 15; this index was significantly smaller,  $\sim 0.4$ , following CHI ( $P < 0.0005$ ) (compare light blue and red curves, Fig. 3*C*), indicating that the new spines in CHI animals added between these two imaging sessions were mostly short-lived. This difference was similar when indexed on days 18 and 25 postinjury ( $P < 0.0005$  and  $P < 0.005$ , respectively). Similarly, spines born between days 13 and 15 and indexed on days 18 and 25 showed a low survival index following CHI (*SI Appendix, Fig. S6*). ISRIB treatment only affected the survival index at day 15 (curves red and dark blue;  $P < 0.05$ ,  $P = 0.7495$ ,  $P = 0.9611$ ), underscoring the notion that spines newly formed after CHI are short-lived and quickly eliminated. ISRIB treatment normalized the number of CHI-induced spines toward control levels. The normalization effect lasted for at least 1 wk after treatment was ended.

**ISR Inhibition Lastingly Reverses Working Memory Deficits Measured after Concussive Injury.** To assess functional consequences of the aberrant spine dynamics measured after CHI in the parietal cortex, we next carried out behavioral experiments



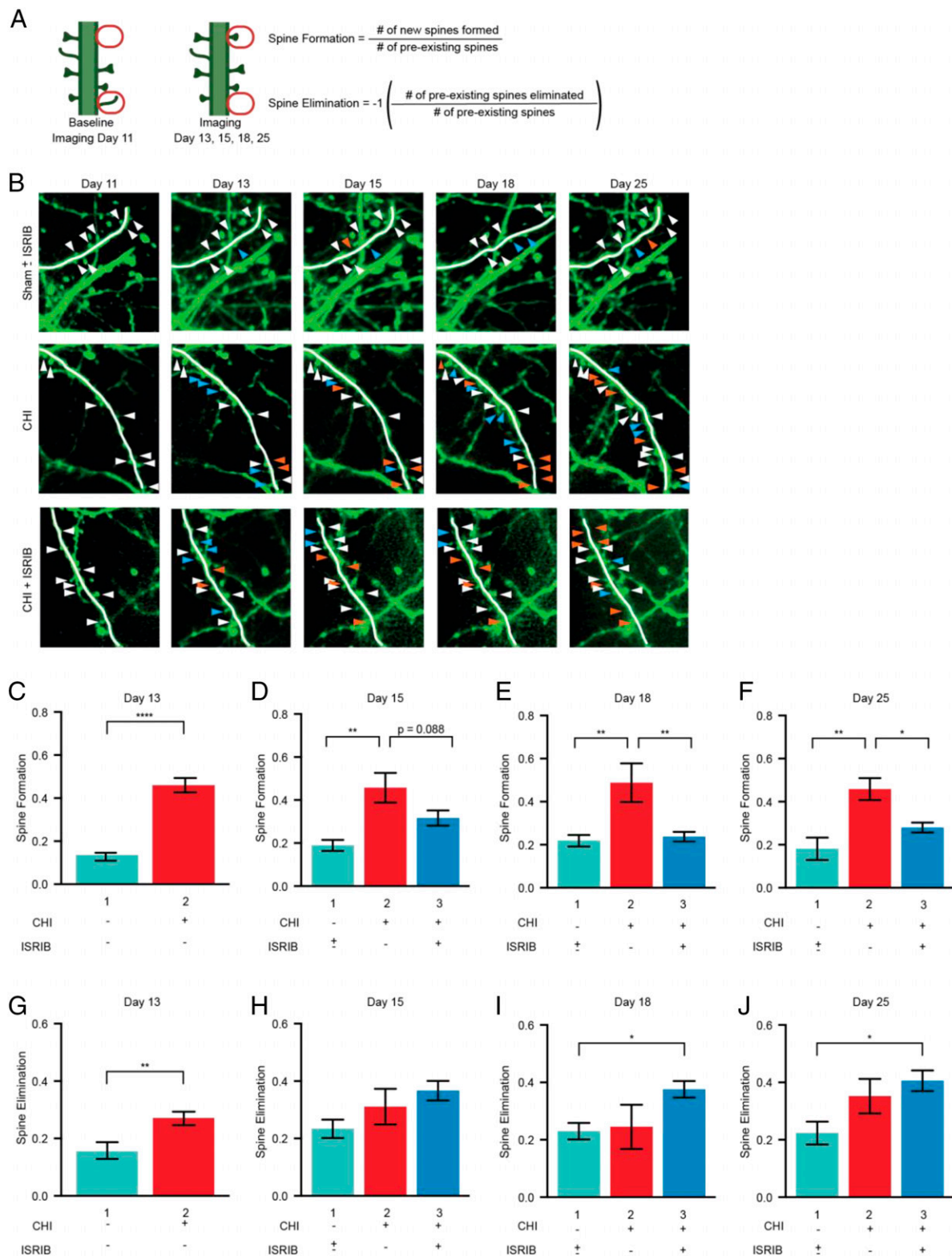


**Fig. 2.** Cortical spine dynamics are altered by concussive injury and restored by ISR inhibition. (A) Analysis schematic depicting how spine formation and spine elimination were scored. Imaging days 13, 15, 18, and 25 were compared to baseline imaging day 11. (B) Representative images. White arrowheads show spines identified on one dendritic segment at baseline; blue arrowheads indicate new spines; orange arrowheads indicate spines that were eliminated. (C–J) Spine formation and spine elimination for  $\pm$  CHI and  $\pm$  ISIRIB treatment. Sham mice that received ISIRIB or Vehicle treatment showed no significant difference and were pooled and graphed as Sham  $\pm$  ISIRIB treatment. Statistics were calculated between the experimental groups and the pooled Sham  $\pm$  ISIRIB treatment. (C) Spine formation at day 13 post-injury (dpi) for sham (Bar 1, cyan) and CHI (Bar 2, red) mice. The number of animals in each group was  $n = 13$  and 23, respectively. (D–F) Spine formation at days 15, 18, and 25 dpi for Sham  $\pm$  ISIRIB (Bar 1) and CHI (Bar 2), and CHI + ISIRIB treatment (Bar 3, blue). ISIRIB treatment had no effect on sham control mice (Supplemental Figure S4). The number of animals in each group was  $n = 13$ , 12, and 11, respectively (note that the 23 animal cohort analyzed in (B) was split into the  $\pm$  ISIRIB groups). (G–J) same as (C–F) but spine elimination was scored. Statistics: Analysis was done by Unpaired *T*-test (C, G) or Ordinary one-way ANOVA followed by multiple comparisons using Tukey-post hoc (D–F, and H–J).  $p < 0.05$  (\*),  $p < 0.005$  (\*\*),  $p < 0.0001$  (\*\*\*\*), as indicated in the figure. All data are means  $\pm$  SEM. Sham  $\pm$  ISIRIB  $n = 13$ ; CHI  $n = 12$ ; CHI + ISIRIB  $n = 11$ .

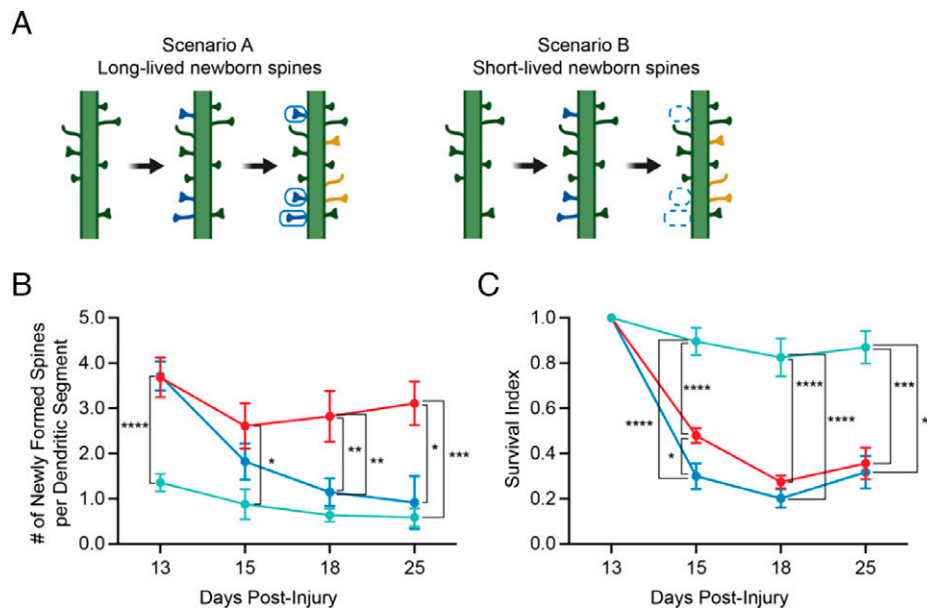


**Fig. 3.** ISR inhibition normalizes the CHI-induced short-lived newborn spines. (A) A schematic illustrating long- vs. short-lived newborn spines. (B) Number of newly formed spines per dendritic segment (dendritic segments were 50–100  $\mu\text{m}$  ( $\pm 2 \mu\text{m}$ ) and were similar in length among groups, Supplemental Table S1) and (C) survival index in Sham  $\pm$  ISRIB (cyan line), CHI (red line), and CHI + ISRIB (blue line) mice (note that the CHI mice were split into the  $\pm$  ISRIB groups) at days 13–25 post-injury (dpi). Sham mice that received ISRIB or Vehicle treatment showed no significant difference and were pooled and graphed as Sham  $\pm$  ISRIB treatment. Statistics were calculated between the experimental groups and the pooled Sham  $\pm$  ISRIB treatment. ISRIB treatment had no effect on sham control mice (data not shown). Statistics: Analysis was done at each dpi by Unpaired *T*-test (B: 13 dpi) or Ordinary one-way ANOVA followed by multiple comparisons using Tukey-post hoc (B: 15–25 dpi, C: 15–25 dpi).  $p < 0.05$  (\*),  $p < 0.005$  (\*\*),  $p < 0.0005$  (\*\*\*),  $p < 0.0001$  (\*\*\*\*), as indicated in the figure. All data are means  $\pm$  SEM. Sham  $\pm$  ISRIB  $n = 13$ ; CHI  $n = 12$ ; CHI + ISRIB  $n = 11$ .

blind to surgical condition and treatment to measure working memory, which is known to depend on parietal cortex function. To this end, we subjected mice to CHI as previously described and measured their performance in the novel object recognition task (NORT). NORT is commonly used to measure working memory in rodents, taking advantage of the mouse's innate preference for novelty (43, 44). Briefly, on days 16 and 17 post-CHI, mice were individually habituated to the measurement arena for 10 min each day and were then exposed on day 18 post-CHI to two identical objects ("learning phase"). Mice were then removed from the arena for 5 min, during which time one of the now familiar objects was replaced with a novel object, and were then returned to the arena to explore and interact with the objects ("testing phase") (blue arrowheads in Fig. 1). Automated tracking software recorded the total interaction time with each object during the learning and testing phases and calculated a "discrimination index" (DI) for each phase [DI = (Time spent with novel – time spent with familiar)/total time]. The DI from the testing phase was used as a metric of working memory function. A high DI score reveals discrimination between the novel and familiar object, and a low DI score indicates impaired discrimination, presumably as a consequence of a defect in working memory.

In the testing phase, CHI mice had a significantly lower DI compared with controls, indicating that CHI induced deficits in working memory ( $P < 0.0005$ ) (compare light blue and red dots, Fig. 4A).

Using the same treatment regimen described above for the spine measurements, we next tested whether ISRIB treatment would reverse the working memory deficits. Remarkably, CHI mice that received ISRIB treatment regained full working memory, with discrimination indistinguishable from that of the control group ( $P = 0.896$ ) (compare light blue and dark blue dots, Fig. 4A). ISRIB treatment did not affect the performance of the control animals (SI Appendix, Fig. S7 and Fig. 4C).

We then repeated the NORT 35 d after the last ISRIB treatment in the same animal cohort but using a different novel object comparable in novelty (blue arrowhead on day 53 in Fig. 1). We observed that CHI mice that had received ISRIB between days 14 and 17 post-CHI maintained full working memory at day 53 ( $P = 0.9911$  not significant[n.s.], comparing DI of day 18 with day 53) (Fig. 4B and E). CHI mice that did not receive ISRIB remained impaired ( $P = 0.3097$  n.s.) (Fig. 4B and D), indicative of long-lasting working memory deficits induced by the CHI. The persistence of the ameliorative effects of ISRIB treatment on working memory deficits induced by CHI for weeks after administration parallels the persistent effects of ISRIB in restoring normal spine dynamics.

## Discussion

We demonstrate here that concussive injury induces aberrant spine dynamics in the parietal cortex that parallels impairments in working memory. Specifically, in each imaging session, we observed a significant increase in spine formation. Newly formed spines, however, were short-lived, as indicated by their short  $\sim 2$ -d lifetime, suggesting that they do not engage in stable, functional synaptic connections. Remarkably, pharmacological inhibition of the ISR with ISRIB reversed the changes in spine dynamics and restored working memory. These restorative effects were maintained weeks after ISRIB treatment was terminated, that is, long after the drug was cleared from the organism. The strong correlation between the anatomical and behavioral findings, including their responses to ISRIB treatment, suggests that structural changes in dendritic spines may be causally linked to cognitive impairments after CHI.

Structural plasticity of dendritic spines is tightly coordinated with synaptic function and neuronal plasticity. For example, spine enlargement parallels long-term potentiation, whereas long-term depression is associated with spine shrinkage (19, 45).

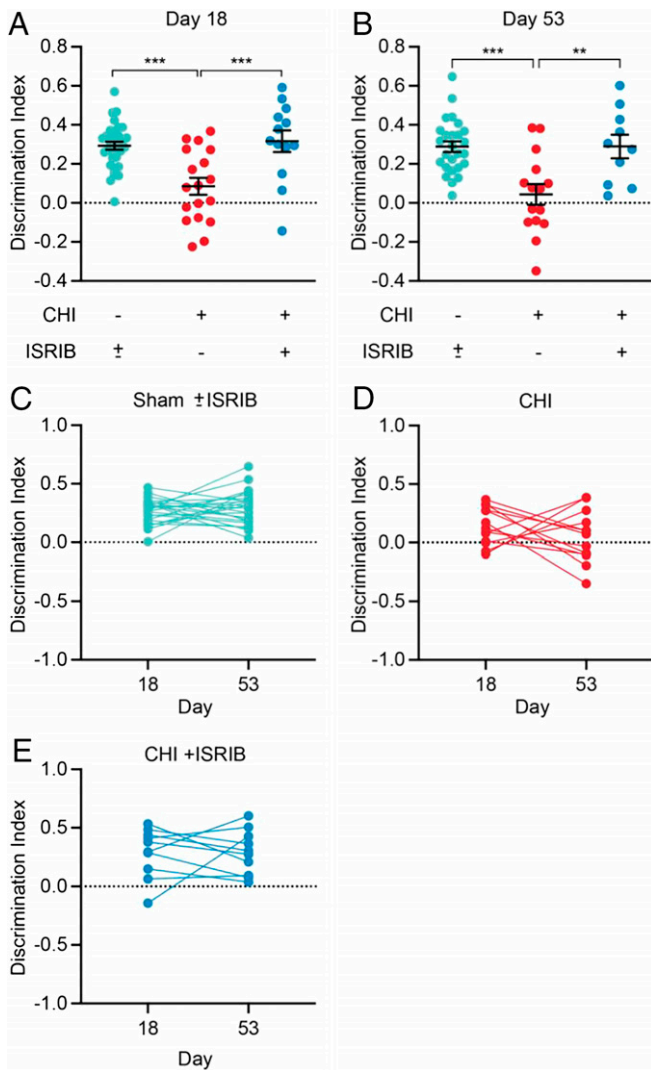


**Fig. 4.** ISR inhibition lastingly reverses working memory deficits measured after concussive injury. Mice were treated as described before and subjected to cognitive testing on days 18 and 53 using NORT (see *Materials and Methods*) as depicted in Figure 1. The habituation phases of the NORT were performed over two days preceding days 18 and 53. (A–B) The discrimination index at day 18 (A) or day 53 (B) for Sham ± ISRIB, CHI, and CHI + ISRIB mice. For both (A) and (B), sham mice that received ISRIB or Vehicle treatment showed no significant difference and were pooled and graphed as Sham ± ISRIB treatment. Statistics were calculated between the experimental groups and the pooled Sham ± ISRIB treatment. ISRIB treatment had no effect on sham control mice (Supplemental Figure S7). (C–E) Connected dot plot comparing the discrimination index for individual animals at days 18 and 53 for Sham ± ISRIB, CHI, and CHI + ISRIB mice. Statistics: Analysis was done by Ordinary one-way ANOVA followed by multiple comparisons using Tukey-post hoc (A–B) or Paired *T*-test (C–E).  $p < 0.005$  (\*\*),  $p < 0.0005$  (\*\*\*), as indicated in the figure. Data in (A) and (B) are means ± SEM. Sham ± ISRIB  $n = 31$ ; CHI  $n = 18$ ; CHI + ISRIB  $n = 13$ .

Changes in dendritic spines can have marked effects on synaptic function, plasticity, and patterns of connectivity in neuronal circuits (18, 24). Notably, disruptions in dendritic spine dynamics, density, or morphology accompany many brain disorders, particularly those that involve deficits in cognitive function (46, 47). Indeed, in an animal model of Huntington’s disease, spine formation increased but newly formed spines did not persist and did not become integrated with the local circuitry (46). Similarly, in mice overexpressing MECP2, a Rett syndrome–related gene, both spine formation and elimination were elevated and new spines were more rapidly eliminated than in wild-type (WT) mice (47).

Altogether, our data are suggestive of an aberrant response that results in the formation of transient spines, as indicated by their short ~2-d lifetime. We speculate that the short-lived spines do not engage in stable, functional synaptic connections and possibly serve as added noise in the circuit, hindering neuronal communication, or as a compensatory mechanism to maximize communication between neurons. Future electron microscopy studies are needed to determine the details of the changes in dendritic spine structure that are associated with cognitive impairment after CHI.

Increasing evidence from animal studies demonstrates that TBI-induced functional deficits are closely related to damage to the synaptic connections of neurons, including dendritic spines (48–50). These studies show an acute reduction in dendritic spine density associated with impaired electrophysiological activity and cognitive function. One study using a pneumatic piston to deliver a single TBI in mice found an acute steady reduction in spine density of layer II/III pyramidal neurons within the parietal cortex (over 1 to 24 h postinjury) that was followed by a slower increase in spine density (at 3 d postinjury) (51). Similarly, in another study analyzing the same region using a fluid percussion injury in rats, spine density declined acutely over 24 h and then returned to control levels within a week postinjury (52). Thus, in each case, an initial acute reduction in spine density was followed by a slower rebounding phase that restored spine density to (or close to) preinjury levels. However, these and other studies remained limited to focal brain injury models, fixed brain tissues, and single-time point analyses. In contrast to previous work, this study used longitudinal imaging *in vivo* to reveal spine dynamics spanning an extended time period after concussive injury when persistent cognitive deficits are measured. Although the injury model, animal, mode of analysis, and time points were different, we also observed the previously noted spontaneous rebound in dendritic spines in CHI. Our mode of analysis spanned an extended time window (spread over an 8- to 15-d period), allowing kinetic characterization of dendritic spine dynamics and density.

Spine imaging was performed on anesthetized mice because of the required mechanical stability when small structures are imaged at diffraction-limited resolution. For events that happen on a scale of days, this is a reasonable approach since the time under anesthesia was short (~1 h) when compared with the time awake between imaging sessions. Thus, the changes observed largely occurred when the animal was awake. Due to the shallow tissue penetration afforded by the two-photon imaging modality, we restricted our analysis to apical dendrites in the superficial layers of the parietal cortex (encompassing the impacted region), where neurons that engage in working memory are positioned close to the brain’s surface.

It remains to be determined whether these observations extend to other neuronal populations and brain regions. Present findings on longitudinal observations of dendritic spines were made on apical tufts of a genetically labeled subset of excitatory neurons in layer V of the cortex. Given that other classes of neurons in different brain regions may have varying spine dynamics, additional investigation is needed to determine whether these findings would be generalizable. Moreover, the causality between aberrant spine dynamics and cognitive dysfunction remains to be determined and warrants further investigation.

Persistent deficits in memory and executive function after TBI have been observed in both humans and animal models (7, 39, 53, 54). Unlike moderate and severe TBI, that is, focal injuries leading to pronounced tissue damage visible by computed

tomography (CT), mild TBI (concussive or repetitive) does not evoke detectable tissue lesions in the brain that can be detected by CT or MRI. However, like severe TBI, mild TBI leads to long-term cognitive dysfunction. The CHI protocol used here resulted in working memory deficits that lasted at least 2 mo after injury.

Despite its high prevalence and impact, the diversity of causes and complexity of injury responses to date have hindered the development of effective treatments to prevent or mitigate deficits associated with TBI (55–58). However, cell-based therapy and enriched environment intervention offer novel approaches to alleviate TBI outcomes (59, 60). In light of this and previous work, drugs targeting spine dynamics now may provide another promising avenue to lessen or alleviate some of the most devastating consequences of the injury (61).

We and others previously showed that both focal and diffuse head injuries, various neurodegenerative diseases, and normal aging all induce phosphorylation of eIF2 $\alpha$  in the brain and thereby activate the ISR (36, 37, 62–65). After TBI, temporary pharmacological inhibition of the ISR with ISRIB completely rescued trauma-induced cognitive and behavioral deficits and neuronal correlates (36, 37). Our observation that ISRIB treatment not only rescued the working memory deficit but also rapidly and persistently reversed aberrant changes in cortical spine dynamics suggests that the link between the ISR and memory function involves at least in part alteration in neuronal structure. In this view, the appearance of transient spines results from ISR activation, which in turn leads to the observed memory deficits because proper synaptic connections are not formed. It will be exciting to next explore whether these observations also extend to the hippocampus, the brain region in which long-term memory consolidation is thought to take place and where similarly remarkable curative effects of ISRIB have been documented.

## Materials and Methods

**Animals.** All experiments were conducted in accordance with NIH Guide for the Care and Use of Laboratory Animals and approved by the Institutional Animal Care and Use Committee of the University of California, San Francisco. Male C57BL/6J WT mice were received from Jackson Laboratories. Male Thy1-YFP-H (in C57 background) were bred in-house. Animals were 10 to 12 wk of age at the time of surgeries. Animal shipments were received at least 1 wk prior to start of experimentation to allow animals to habituate to the new surroundings. Mice were group-housed in environmentally controlled conditions with a reverse light cycle (12:12 h light:dark cycle at  $21 \pm 1^\circ\text{C}$ ;  $\sim 50\%$  humidity) and provided food and water ad libitum. Behavioral analysis was performed during the dark cycle.

**CHI and Sham Surgery.** Mice (10- to 12-wk-old C57BL/6J or Thy1-YFP-H in C57 background) were randomly assigned to the CHI or sham surgery group. Animals were anesthetized and maintained at 2 to 2.5% isoflurane during surgery. Animals were secured to a stereotaxic frame with nontraumatic ear bars. The head of the animal was supported with a foam pad before injury. Contusion was induced using a 5-mm convex tip attached to an electromagnetic impactor (Leica) at the following coordinates: anteroposterior,  $-1.50$  mm and mediolateral,  $0$  mm with respect to bregma. Contusion was produced with an impact depth of 1 mm from the surface of the skull with a velocity of 5.0 m/s sustained for 300 ms. No animals had a fractured skull after injury. Sham animals were secured to a stereotaxic frame with nontraumatic ear bars and received the midline skin incision but no impact. After CHI or sham surgery, the scalp was sutured, and the animal was allowed to recover in an incubation chamber set to  $37^\circ\text{C}$ . All animals recovered from the surgical procedures as exhibited by normal behavior and weight maintenance monitored throughout the duration of the experiments.

**Drug Administration.** ISRIB solution was made as previously described in ref. 63. Stock ISRIB solution was at 0.1 mg/mL and was injected at a dose of 2.5 mg/kg.

**Headplate and Cranial Window Attachment Surgery.** Mice (10- to 12-wk-old Thy1-YFP-H in C57 background) underwent headplate and cranial window attachment surgery. Animals were anesthetized, maintained at 1.5% isoflurane, and placed over a protected thermal plate ( $37^\circ\text{C}$ ) during surgery. Animals were secured to a stereotaxic frame with nontraumatic ear bars. After anesthesia induction, dexamethasone (intraperitoneal), meloxicam (intraperitoneal), and lidocaine (subcutaneous) drugs were administered. The scalp was cleaned with ethanol 70% and disinfected with betadine, and the skull was exposed with a midline scalp incision. A craniotomy was performed on the right parietal cortex with a high-speed drill equipped with a round bur. To avoid damaging the underlying cortex by friction-induced heat, a cool sterile solution was added to the skull periodically, and drilling was intermittent to permit heat dissipation. The excised skull was replaced by a 3-mm coverslip window (Harvard Apparatus, Round Cover Glass) carefully positioned on top of the brain and secured against the skull with tissue adhesive (3M Vetbond tissue adhesive). A custom-made headplate with a central opening was attached with dental cement (Parkell C&B Metabond Quick Adhesive Cement System). After the surgery, the animal was allowed to recover in an incubation chamber set to  $37^\circ\text{C}$  before returning to its home cage. All animals recovered from the surgical procedures as exhibited by normal behavior and weight maintenance monitored throughout the duration of the experiments. Animals were allowed to recover before the start of imaging experiments.

**Transcranial Two-Photon Imaging In Vivo.** Transcranial two-photon imaging was performed in vivo using a movable objective microscope manufactured by the Sutter Instrument Company. A mode-locked Ti:Sapphire laser (Chameleon Ultra 2; Coherent, Inc.) was tuned to 920 nm, and the laser power through the objective was adjusted within the range of 60 to 80 mW. Emission light was collected by a 40x water-immersion objective (NA0.8; IR2; Olympus), filtered by emission filters (525/70 and 610/75 nm; Chroma Technology), and measured by two independent photomultiplier tubes (Hamamatsu; R3896). Scanning and image acquisition of apical dendrites in layer I/II of layer V pyramidal neurons expressing green fluorescent protein was controlled by ScanImage software (Vidrio Technologies). Z-stacks were collected with a step size of 1  $\mu\text{m}$  in the z axis and the pixel size to 0.1513  $\mu\text{m}$ . Each slice of the stack was obtained by averaging 25 frames. Mice were imaged for four or five sessions over an 8- or 15-d period. Care was taken with each imaging session to achieve similar fluorescence levels. Mice were held under isoflurane anesthesia (1.5% in oxygen) for 1 h with head fixed during structural imaging. The body temperature of the mouse was kept at  $37^\circ\text{C}$  using a feedback-controlled electric heating pad.

**Spine Dynamics Analysis.** For spine dynamics analysis, image stacks collected on days 13, 15, 18, and 25 were first aligned to their corresponding baseline imaging stack collected on day 11 using the CMTK Registration Gui plugin to NIH ImageJ/FIJI software (66, 67). Spine formation and elimination analysis was done semiautomated using the NIH FIJI software to save the X, Y, Z coordinates of identified spines on traced dendrites from regions of interest (ROI) in the day 11 image stacks. The X, Y, Z coordinates were then applied to image stacks from subsequent imaging sessions to note the continued presence or disappearance of preexisting spines or the presence of a new spine. Spine formation and elimination were graphed as compared with baseline imaging on day 11, and 40 to 57 dendrites ranging between 50 to 100  $\mu\text{m}$  ( $\pm 2$   $\mu\text{m}$ ) in length were analyzed per mouse and then averaged. A total length of at least 3,500  $\mu\text{m}$  of dendrites and 200 to 600 spines were analyzed per experimental group. To exclude the possibility that the measured changes analyzed were due to the choice of day 11 as the baseline for analysis, spine formation and elimination were analyzed in reverse by comparing days 11, 13, and 15 with day 18. Spine dynamics analysis was done semiautomated, blinded to surgical condition and therapeutic intervention, and cross-checked by a separate investigator. Data reported are the average of the counts by multiple investigators.

The number of new spines formed per imaging session was quantified by noting the number of new spines formed per dendritic segment (first observed) at imaging days 13, 15, and 18. Multiple dendrites were analyzed per mouse



and averaged. Lengths of the dendritic segments analyzed were similar among groups (SI Appendix, Table S1).

To calculate the survival index, we determined the number of spines present at subsequent imaging sessions divided by the number of spines present when first observed. First, individual spines were classified as  $S_{11}$ ,  $S_{13}$ ,  $S_{15}$ , or  $S_{18}$  depending on which imaging day they were first observed. Next, a binary system was used to denote presence (indicated by a 1) or not (indicated by a 0) across the imaging sessions. In this scale, a survival index closer to 1 denotes long-lived and a survival index closer to 0 denotes short-lived. For every dendrite, the survival index was calculated for each dendritic spine population ( $S_{11}$ ,  $S_{13}$ ,  $S_{15}$ , or  $S_{18}$ ). The average survival index of each dendritic spine population was graphed per mouse.

**Spine Density Quantification.** For spine density analysis (number of spines per micrometer of dendritic length), we determined the total number of spines present at baseline imaging day 11 divided by the total number of spines present at each subsequent imaging session per dendrite. All protrusions greater than 0.55  $\mu\text{m}$  from a dendrite were counted as spines regardless of morphology. The average spine density at each imaging session was graphed per mouse. Spine density analysis was done semiautomated, blinded to surgical condition and therapeutic intervention, and cross-checked by a separate investigator. Data reported are the average of the counts by multiple investigators.

**Tissue Collection.** Mice were lethally overdosed using a mixture of ketamine (10 mg/mL) and xylazine (1 mg/mL). Once animals were completely anesthetized, blood was extracted by cardiac puncture and animals were perfused with 1X phosphate buffer solution (PBS), pH 7.4 (Gibco; Big Cabin OK, -70011-044) until the livers were clear ( $\sim 1$  to 2 min). For measurements of drug concentration following PBS perfusion, the whole brain was rapidly removed, and a hemibrain was dissected and weighed, snap frozen on dry ice, and stored at  $-80^\circ\text{C}$  until processing.

**Immunohistochemistry Analysis and Quantification.** For immunohistochemistry analysis following PBS perfusion, whole brains were fixed in ice-cold 4% paraformaldehyde, pH 7.5 (Sigma Aldrich; 441244) for 4 h followed by sucrose (Fisher Science Education; S25590A) protection (15 to 30%). Brains were embedded with 30% sucrose/Optimal Cutting Temperature Compound (Tissue Tek; 4583) mixture on dry ice and stored at  $-80^\circ\text{C}$ . Brains were sectioned into 20- $\mu\text{m}$  slides using a Leica cryostat (Leica Microsystems) and mounted on slides (Thermo Fisher Scientific). Slides were brought to room temperature ( $20^\circ\text{C}$ ) prior to use. Slides were washed in Tris buffered saline (TBS) Tween solution for 10 min and twice with TBS for 10 min each. All slides were blocked in Block Reagent (Perkin-Elmer; FP1020) for 30 min in the dark. Slides were stained with primary antibodies specific for NeuN (Rabbit, Abcam; ab128886) overnight, washed three times in TBS, and stained for the secondary antibody, goat anti-rabbit Alexa-568 (Invitrogen; A-11011). Tissues were fixed using ProLong Gold (Invitrogen; P36930) and a standard slide cover sealed with nail polish. Three or four images separated by 60 to 140  $\mu\text{m}$  in the cortex were averaged per animal. A Zeiss Axio Imager Z1 fluorescence scope was used at 10x and 20x magnification to acquire 15  $\mu\text{m}$  z-stack images at a slice interval of 0.5  $\mu\text{m}$ . Quantitative analysis was performed using NIH FIJI analysis software (v1.52n). Neurons were determined using the neuronal marker (NeuN). The neuronal numbers were determined by quantification of neuronal nuclei and by image-covering staining and expressed as total numbers or percentage of the total area.

**Novel Object Recognition Task with 5-min Retention Interval.** For all behavioral assays, the experimenters were blinded to treatment and surgical condition. Prior to behavioral analysis, animals were inspected for gross motor impairments. Animals were inspected for whisker loss, limb immobility

(including grip strength), and eye occlusions. If animals displayed any of these impairments, they were excluded. Behavioral assessment was recorded and scored using a video tracking and analysis setup (Ethovision XT 8.5; Noldus Information Technology).

The novel objective recognition task was modified from a previously described protocol (68). The task took place during the dark cycle in a room with dim red light. Mice were individually habituated in a 30 cm  $\times$  30 cm  $\times$  30 cm (L $\times$ W $\times$ H) opaque Plexiglas box (termed "arena") for 10 min per day for 2 d preceding the test. On the third day, mice were exposed to two identical objects for 5 min (learning phase). The mice were then temporarily removed for 5 min to allow for one of the objects to be replaced by a novel object. Mice were then returned to the arena for 5 min to explore and interact with the objects (testing phase). In each experiment, the location of the novel object was randomly selected between the left and right sides to avoid side-preference bias. Mouse behavior was recorded with an overhead video camera; the video files were exported for analysis. Data are presented as a DI, calculated using the formula  $DI = [(Time\ spent\ with\ novel - time\ spent\ with\ familiar)/total\ time]$ .

Animals were injected (intraperitoneal) with either vehicle or ISRIB (2.5 mg/kg) starting 2 d before the first training day (days 14 and 15 postinjury) (Fig. 1) and after each of the habituation days (days 16 and 17 postinjury) for a total of four doses. No injections were given when working memory was tested on day 18 postinjury or thereafter. On day 53 (that is, 35 d after the last ISRIB/vehicle treatment), we measured working memory as described above but used a different novel object comparable in novelty.

**Statistical Analysis.** All data were analyzed with GraphPad Prism 9 statistical software. Analyses were done using unpaired *t* test, one-way analysis of variance (ANOVA), and two-way repeated-measures ANOVA (individual statistical tools and post hoc analyses denoted in the figure legends). *P* values of  $<0.05$  were considered significant. Individual animal scores are represented by dots, and lines depict data means  $\pm$  SEM. Group outliers were determined (GraphPad Software Outlier Test-Grubb's test) and excluded from analysis. At most, a single animal was excluded from each experimental cohort.

**Data, Materials, and Software Availability.** All data are included in the main text and figures and in the supplemental information (SI). Code used in the analysis is available at the sites noted in the text and references.

**ACKNOWLEDGMENTS.** This work was supported by NIH Grants R01AG056770 (S.R.) and R01EY002874 and R01MH122478 (M.P.S.); NSF Grant 1822650 (M.P.S.); the generous support of the Rogers family to S.R. and P.W.; and the Weill Innovation Award to S.R. and P.W. P.W. is an Investigator of the HHMI. E.S.F. was supported by the National Institute of General Medical Sciences Initiative for Maximizing Student Development Fellowship Program (IMSD R25GM056847) and the NSF Graduate Research Fellowship Program (GRFP 2034836). Findings in this manuscript were submitted by E.S.F. in partial fulfillment of the requirements for a PhD at University of California, San Francisco. Figs. 1, 2A, and 3A were created with [Biorender.com](https://biorender.com).

Author affiliations: <sup>a</sup>Department of Physical Therapy and Rehabilitation, University of California, San Francisco, CA 94143; <sup>b</sup>Brain and Spinal Injury Center, University of California, San Francisco, CA 94143; <sup>c</sup>Department of Physiology, University of California, San Francisco, CA 94143; <sup>d</sup>Department of Translational Research, Protein Folding and Disease Laboratory, Fundación Ciencia & Vida, Santiago, 7750000, Chile; <sup>e</sup>Department of Biochemistry and Biophysics, University of California, San Francisco, CA 94143; <sup>f</sup>HHMI, University of California, San Francisco, CA 94143; <sup>g</sup>Kavli Institute of Fundamental Neuroscience, University of California, San Francisco, CA 94143; <sup>h</sup>Department of Neurological Surgery, University of California, San Francisco, CA 94143; and <sup>i</sup>Weill Institute for Neuroscience, University of California, San Francisco, CA 94143

1. S. R. Flanagan, Invited commentary on "Centers for Disease Control and Prevention report to Congress: Traumatic brain injury in the United States: Epidemiology and rehabilitation." *Arch. Phys. Med. Rehabil.* **96**, 1753–1755 (2015).
2. C. A. Taylor, J. M. Bell, M. J. Breiding, L. Xu, Traumatic brain injury-related emergency department visits, hospitalizations, and deaths—United States, 2007 and 2013. *MMWR Surveill. Summ.* **66**, 1–16 (2017).
3. J. H. Cole, R. Leech, D. J. Sharp, Alzheimer's Disease Neuroimaging Initiative, Prediction of brain age suggests accelerated atrophy after traumatic brain injury. *Ann. Neurol.* **77**, 571–581 (2015).

4. Y. Li *et al.*, Head injury as a risk factor for dementia and Alzheimer's disease: A systematic review and meta-analysis of 32 observational studies. *PLoS One* **12**, e0169650 (2017).
5. B. E. Masel, D. S. DeWitt, Traumatic brain injury: A disease process, not an event. *J. Neurotrauma* **27**, 1529–1540 (2010).
6. S. P. Broglio, J. T. Eckner, H. L. Paulson, J. S. Kutcher, Cognitive decline and aging: The role of concussive and subconcussive impacts. *Exerc. Sport Sci. Rev.* **40**, 138–144 (2012).
7. B. C. McDonald, L. A. Flashman, A. J. Saykin, Executive dysfunction following traumatic brain injury: Neural substrates and treatment strategies. *NeuroRehabilitation* **17**, 333–344 (2002).

8. W. J. Chai, A. I. Abd Hamid, J. M. Abdullah, Working memory from the psychological and neurosciences perspectives: A review. *Front. Psychol.* **9**, 401 (2018).
9. J. Eriksson, E. K. Vogel, A. Lansner, F. Bergström, L. Nyberg, Neurocognitive architecture of working memory. *Neuron* **88**, 33–46 (2015).
10. S. Funahashi, Working memory in the prefrontal cortex. *Brain Sci.* **7**, 49 (2017).
11. M. Mayford, S. A. Siegelbaum, E. R. Kandel, Synapses and memory storage. *Cold Spring Harb. Perspect. Biol.* **4**, a005751 (2012).
12. J. J. Langille, R. E. Brown, The synaptic theory of memory: A historical survey and reconciliation of recent opposition. *Front. Syst. Neurosci.* **12**, 52 (2018).
13. A. Citri, R. C. Malenka, Synaptic plasticity: Multiple forms, functions, and mechanisms. *Neuropsychopharmacology* **33**, 18–41 (2008).
14. M. D. Amaral, L. Pozzo-Miller, The dynamics of excitatory synapse formation on dendritic spines. *Cellscience* **5**, 19–25 (2009).
15. K. O. Lai, N. Y. Ip, Structural plasticity of dendritic spines: The underlying mechanisms and its dysregulation in brain disorders. *Biochim. Biophys. Acta* **1832**, 2257–2263 (2013).
16. H. Steffens *et al.*, Stable but not rigid: Chronic in vivo STED nanoscopy reveals extensive remodeling of spines, indicating multiple drivers of plasticity. *Sci. Adv.* **7**, eabf2806 (2021).
17. C. Sala, M. Segal, Dendritic spines: The locus of structural and functional plasticity. *Physiol. Rev.* **94**, 141–188 (2014).
18. E. A. Nimchinsky, B. L. Sabatini, K. Svoboda, Structure and function of dendritic spines. *Annu. Rev. Physiol.* **64**, 313–353 (2002).
19. Y. Nakahata, R. Yasuda, Plasticity of spine structure: Local signaling, translation and cytoskeletal reorganization. *Front. Synaptic Neurosci.* **10**, 29 (2018).
20. R. Yasuda, Biophysics of biochemical signaling in dendritic spines: Implications in synaptic plasticity. *Biophys. J.* **113**, 2152–2159 (2017).
21. J. Tønnesen, G. Katona, B. Rózsa, U. V. Nägerl, Spine neck plasticity regulates compartmentalization of synapses. *Nat. Neurosci.* **17**, 678–685 (2014).
22. K. P. Berry, E. Nedivi, Spine dynamics: Are they all the same? *Neuron* **96**, 43–55 (2017).
23. G. Yang, F. Pan, W. B. Gan, Stably maintained dendritic spines are associated with lifelong memories. *Nature* **462**, 920–924 (2009).
24. C. H. Bailey, E. R. Kandel, K. M. Harris, Structural components of synaptic plasticity and memory consolidation. *Cold Spring Harb. Perspect. Biol.* **7**, a021758 (2015).
25. M. U. Ghani *et al.*, Dendritic spine classification using shape and appearance features based on two-photon microscopy. *J. Neurosci. Methods* **279**, 13–21 (2017).
26. M. Adrian *et al.*, Barriers in the brain: Resolving dendritic spine morphology and compartmentalization. *Front. Neuroanat.* **8**, 142 (2014).
27. A. Holtmaat *et al.*, Long-term, high-resolution imaging in the mouse neocortex through a chronic cranial window. *Nat. Protoc.* **4**, 1128–1144 (2009).
28. J. Grutzendler, N. Kasthuri, W. B. Gan, Long-term dendritic spine stability in the adult cortex. *Nature* **420**, 812–816 (2002).
29. B. Lendvai, E. A. Stern, B. Chen, K. Svoboda, Experience-dependent plasticity of dendritic spines in the developing rat barrel cortex in vivo. *Nature* **404**, 876–881 (2000).
30. J. T. Trachtenberg *et al.*, Long-term in vivo imaging of experience-dependent synaptic plasticity in adult cortex. *Nature* **420**, 788–794 (2002).
31. C. C. Chen, J. Lu, Y. Zuo, Spatiotemporal dynamics of dendritic spines in the living brain. *Front. Neuroanat.* **8**, 28 (2014).
32. M. Costa-Mattioli, P. Walter, The integrated stress response: From mechanism to disease. *Science* **368**, eaat5314 (2020).
33. H. P. Harding *et al.*, An integrated stress response regulates amino acid metabolism and resistance to oxidative stress. *Mol. Cell* **11**, 619–633 (2003).
34. N. Donnelly, A. M. Gorman, S. Gupta, A. Samali, The eIF2 $\alpha$  kinases: Their structures and functions. *Cell. Mol. Life Sci.* **70**, 3493–3511 (2013).
35. O. J. Freeman, G. R. Mallucci, The UPR and synaptic dysfunction in neurodegeneration. *Brain Res.* **1648** (Pt B), 530–537 (2016).
36. A. Chou *et al.*, Inhibition of the integrated stress response reverses cognitive deficits after traumatic brain injury. *Proc. Natl. Acad. Sci. U.S.A.* **114**, E6420–E6426 (2017).
37. K. Krukowski *et al.*, Integrated stress response inhibitor reverses sex-dependent behavioral and cell-specific deficits after mild repetitive head trauma. *J. Neurotrauma* **37**, 1370–1380 (2020).
38. G. Feng *et al.*, Imaging neuronal subsets in transgenic mice expressing multiple spectral variants of GFP. *Neuron* **28**, 41–51 (2000).
39. C. N. Bodnar, K. N. Roberts, E. K. Higgins, A. D. Bachstetter, A systematic review of closed head injury models of mild traumatic brain injury in mice and rats. *J. Neurotrauma* **36**, 1683–1706 (2019).
40. Y. Zuo, A. Lin, P. Chang, W. B. Gan, Development of long-term dendritic spine stability in diverse regions of cerebral cortex. *Neuron* **46**, 181–189 (2005).
41. C. Sidrauski *et al.*, Pharmacological brake-release of mRNA translation enhances cognitive memory. *eLife* **2**, e00498 (2013).
42. T. Xu *et al.*, Rapid formation and selective stabilization of synapses for enduring motor memories. *Nature* **462**, 915–919 (2009).
43. L. M. Lueptow, Novel object recognition test for the investigation of learning and memory in mice. *J. Vis. Exp.* **126**, 55718 (2017).
44. M. Antunes, G. Biala, The novel object recognition memory: Neurobiology, test procedure, and its modifications. *Cogn. Process.* **13**, 93–110 (2012).
45. H. Kasai, M. Fukuda, S. Watanabe, A. Hayashi-Takagi, J. Noguchi, Structural dynamics of dendritic spines in memory and cognition. *Trends Neurosci.* **33**, 121–129 (2010).
46. R. P. Murmu, W. Li, A. Holtmaat, J. Y. Li, Dendritic spine instability leads to progressive neocortical spine loss in a mouse model of Huntington's disease. *J. Neurosci.* **33**, 12997–13009 (2013).
47. M. Jiang *et al.*, Dendritic arborization and spine dynamics are abnormal in the mouse model of MECP2 duplication syndrome. *J. Neurosci.* **33**, 19518–19533 (2013).
48. C. N. Winston *et al.*, Controlled cortical impact results in an extensive loss of dendritic spines that is not mediated by injury-induced amyloid-beta accumulation. *J. Neurotrauma* **30**, 1966–1972 (2013).
49. W. A. Ratliff, V. Delic, C. G. Pick, B. A. Citron, Dendritic arbor complexity and spine density changes after repetitive mild traumatic brain injury and neuroprotective treatments. *Brain Res.* **1746**, 147019 (2020).
50. X. Gao, P. Deng, Z. C. Xu, J. Chen, Moderate traumatic brain injury causes acute dendritic and synaptic degeneration in the hippocampal dentate gyrus. *PLoS One* **6**, e24566 (2011).
51. C. N. Winston *et al.*, Dendritic spine loss and chronic white matter inflammation in a mouse model of highly repetitive head trauma. *Am. J. Pathol.* **186**, 552–567 (2016).
52. J. N. Campbell, D. Register, S. B. Churn, Traumatic brain injury causes an FK506-sensitive loss and an overgrowth of dendritic spines in rat forebrain. *J. Neurotrauma* **29**, 201–217 (2012).
53. C. H. Salmund, B. J. Sahakian, Cognitive outcome in traumatic brain injury survivors. *Curr. Opin. Crit. Care* **11**, 111–116 (2005).
54. O. Zohar *et al.*, Closed-head minimal traumatic brain injury produces long-term cognitive deficits in mice. *Neuroscience* **118**, 949–955 (2003).
55. R. Vink, A. J. Nimmo, Multifunctional drugs for head injury. *Neurotherapeutics* **6**, 28–42 (2009).
56. S. Y. Ng, A. Y. W. Lee, Traumatic brain injuries: Pathophysiology and potential therapeutic targets. *Front. Cell. Neurosci.* **13**, 528 (2019).
57. D. S. DeWitt *et al.*, Pre-clinical testing of therapies for traumatic brain injury. *J. Neurotrauma* **35**, 2737–2754 (2018).
58. S. Margulies *et al.*, Combination therapies for traumatic brain injury: Retrospective considerations. *J. Neurotrauma* **33**, 101–112 (2016).
59. M. Galgano *et al.*, Traumatic brain injury: Current treatment strategies and future endeavors. *Cell Transplant.* **26**, 1118–1130 (2017).
60. M. Monsour, D. Ebedes, C. V. Borlongan, A review of the pathology and treatment of TBI and PTSD. *Exp. Neurol.* **351**, 114009 (2022).
61. Y. Xiong, A. Mahmood, M. Chopp, Remodeling dendritic spines for treatment of traumatic brain injury. *Neural Regen. Res.* **14**, 1477–1480 (2019).
62. G. Zhang, X. Wang, B. A. Rothermel, S. Lavandro, Z. V. Wang, The integrated stress response in ischemic diseases. *Cell Death Differ.* **29**, 750–757 (2022).
63. K. Krukowski *et al.*, Small molecule cognitive enhancer reverses age-related memory decline in mice. *eLife* **9**, e62048 (2020).
64. S. Bond, C. Lopez-Lloreda, P. J. Gannon, C. Akay-Espinoza, K. L. Jordan-Sciutto, The integrated stress response and phosphorylated eukaryotic initiation factor 2 $\alpha$  in neurodegeneration. *J. Neuropathol. Exp. Neurol.* **79**, 123–143 (2020).
65. T. Ma *et al.*, Suppression of eIF2 $\alpha$  kinases alleviates Alzheimer's disease-related plasticity and memory deficits. *Nat. Neurosci.* **16**, 1299–1305 (2013).
66. G. Jefferis, Computational morphometry toolkit (CMTK): Tool/resource info (2009). <https://www.nitrc.org/projects/cmtk>. Accessed 2 June 2022.
67. G. Jefferis, Simple GUI frontend for CMTK image registration tools in Fiji/ImageJ (2009). <https://github.com/jefferis/fiji-cmtk-gui>. Accessed 2 June 2022.
68. X. Feng *et al.*, Colony-stimulating factor 1 receptor blockade prevents fractionated whole-brain irradiation-induced memory deficits. *J. Neuroinflammation* **13**, 215 (2016).